Final Report
Mapping *Phragmites*

Project Members
Utah Department of Natural Resources - Division of Forestry, Fire and State Lands (DNR-FFSL)
Erik Neemann
30 April 2019

Introduction

The invasive species *Phragmites australis*, or common reed, causes numerous problems in Utah wetlands, including along the shores of the Great Salt Lake. The tall reed grows very densely into invaded regions (Figure 1), spreading through a horizontal, underground root system comprised of rhizomes, and reproducing via wind-blown seed dispersal (Michigan Department of Natural Resources, 2014). Because it is such a hearty and resilient plant, it crowds out native wetland species, disrupts migratory bird habitats, negatively impacts recreation, and alters the surface water regime, often converting submerged or saturated soils to dry land. In 2014, it was estimated that *Phragmites* occupied nearly 23,000 acres of wetland along the Great Salt Lake shoreline (Long, 2014). As a result, the Utah Department of Natural Resources, Division of Forestry, Fire, and State Lands (FFSL), has taken an aggressive approach to mitigating the *Phragmites* problem. Mitigation activities can include everything from cutting and crushing to burning and flooding. Another big component of *Phragmites* mitigation along the Great Salt Lake includes spraying a wetland-safe chemical to kill the plant in order to allow native species to return (Figure 2). Spraying can be conducted effectively and efficiently with automated, GPS-enabled spraying equipment but accurate geographic data containing the location and boundary of *Phragmites* areas is currently unavailable. Recent research indicates that remotely sensed imagery, from a variety of platforms, may provide a means for identifying the location of *Phragmites* in wetland scenes (Lantz, 2012; Samiappan, 2017; Zhang, 2018). This project aims to automate *Phragmites* mapping from satellite and unmanned aerial system (UAS) imagery, using a prototype Python script.

Methodology

Remotely sensed imagery was collected from three different platforms to be used in a supervised classification algorithm. In order to compare the performance across different spatial resolutions and spectral bands, a diverse mix of imagery was chosen. The image platforms include the European Space Agency's Sentinel-2 satellite, DigitalGlobe's World-View 2 (WV-2) satellite, and PMG Vegetation's UAS (Table 1). PMG Vegetation is a vegetation control company that FFSL has contracted with to perform *Phragmites* mitigation activities. They provided red, green, blue (RGB; ~660 nm, 550 nm, and 480 nm wavelengths, respectively) imagery captured from a DJI Matrice 200 series UAS. The Sentinel-2 imagery was acquired via Google Earth Engine and the DigitalGlobe imagery was downloaded from their webpage with Utah DNR's account. Each of these platforms collects imagery in different wavelength bands and spatial resolutions, as shown in Table 1. The study initially included three areas along the eastern shore of the Great Salt Lake, but was narrowed down to just the Howard Slough Waterfowl Management Area, because it was the only location with available UAS imagery (Figure 3). The footprint of the UAS image covers approximately 538 acres, while the larger rectangular region used for the satellite imagery covers 996 acres. The Sentinel-2 and UAS imagery was collected in late-

September 2018, while the WorldView-2 imagery is from mid-July 2018. For the simplicity, all three images were treated as if they were collected on the same date.

Sufficient ground reference vegetation and land cover data were not available from the time of imagery collection, so a shapefile containing reference land cover polygons was manually generated through visual interpretation of the high-resolution imagery. All reference polygons were located within the footprint of the UAS image and were used for training and validation on imagery from all three platforms.

The images were processed with a Python 3 script that primarily leverages open-source software libraries, with the exception of the ArcPy library, which was installed with ESRI's ArcGIS Pro. The overall script workflow is broken into several main steps, as depicted in Figure 4. First, the script loads each image as a multi-band raster, using wavelength bands available to the specific platform. For the UAS image, only RGB bands are available, while the Sentinel-2 and WorldView-2 images utilize, red edge (~730 nm), and near infrared (~840) bands in addition to the RGB bands. In the second step, additional bands are calculated to provide more variables to the classification algorithm. The normalized difference vegetation index (NDVI) and normalized difference water index (NDWI) are calculated for Sentinel-2 and WorldView-2 images that have the near infrared band. Further, two texture measures, dissimilarity and contrast are calculated for all three platforms using the red band and a 7x7 pixel moving window. In the third step, the reference land cover polygons are loaded as a raster, matching the grid and resolution of the image being process. This means the reference data are loaded at a different resolution for each platform, which has impacts that must be considered when assessing classification performance. In the fourth step, the image is passed into a segmentation algorithm, called quick shift (Vedaldi & Soatto, 2008), which breaks it into objects with similar spectral characteristics. The fifth step then uses those image objects to calculate band-averages for each object with ArcPy's zonal statistics function. In the sixth step, the reference land cover data are split into training (75%) and validation (25%) data sets. The training data are then used to train a random forest classifier model that employs bootstrap sampling and random parameter selection. Random forest is a machine-learning classifier that builds an ensemble of decision trees to determine the most appropriate class for each object (Breiman, 2001). The seventh step, the trained random forest model is applied to predict the land cover class of each image object. Finally, in the last step of the script workflow, the boundaries of the *Phragmites* land cover class are identified and exported as a shapefile. The resulting shapefile can then be ingested by GPS-enabled spraying equipment to conduct targeted *Phragmites* mitigation.

Objective metrics were calculated to evaluate the performance of the classified images. A confusion matrix was computed for each image, including the overall accuracy and Cohen's Kappa. User's and Producer's accuracies were also calculated to compare performance across classes. These metrics were all generated from the validation data set, which was comprised of 25% of ground reference data. Finally, an "out-of-bag" overall accuracy was computed, which used the training pixels that were not selected by the bootstrapping algorithm in the random forest classifier's training phase, and therefore remained independent.

Results and Discussion

Subjectively, the final classified images from each of the platforms show quite different results (Figure 5). The Sentinel-2 image consists of fewer, larger objects than the other two platforms, related to the larger pixel size and same parameters that were used across all three platforms in the image segmentation algorithm. The classification has a relatively large patch of water in the center of the UAS footprint (hereafter referred to simply as "footprint") with an even larger area of native emergent vegetation in the west-central portion of the footprint. *Phragmites* appears to be generally overclassified, which also seems to be the case for the other two platforms. The Sentinel-2 image does appear to do a good job of identifying the dead *Phragmites* area in the northeast corner of the image, primarily outside of the footprint. This dead *Phragmites* region is not present in the WorldView-2 image, which was taken about ten weeks earlier in mid-July, and is correctly classified as live *Phragmites*. The WorldView-2 image also has much more coverage of dead *Phragmites* and bare ground classes than the other two platforms, particularly in the southeast corner of the image. The mowed stripe along the eastern edge of the footprint clearly stands out and appears accurately classified as dead *Phragmites* or bare ground. Of note, there are very few objects that were classified as native emergent vegetation in the WorldView-2 image. This is also depicted in the confusion matrix (Figure 6b), where native emergent was often misclassified as live *Phragmites*, with one of the lowest Producer's accuracies among all classes and platforms at 0.57. The UAS image had by far the most numerous and smallest objects of any platform, resulting in a speckled appearance where small patches of classes dot the landscape of otherwise homogeneous regions. Contrasting with the WorldView-2 image, the UAS image has much greater coverage of the native emergent class, but almost no bare ground objects. The bare ground almost exclusively appears along the road on the northern edge of the image, where the training polygons were present. All three platforms seem to have a reasonable depiction of the triangle-shaped area of dead *Phragmites* in the far northwest corner of the footprint. A very high percentage of the live *Phragmites* class was also present in all three images: 66.1% of all Sentinel-2 pixels, 61.1% of WorldView-2 pixels, and 75.8% of UAS pixels.

Although the classified images demonstrate visibly different results across the platforms, each platform scored quite well on the objective metrics that were calculated (Table 2). The Sentinel-2 image's overall accuracy and kappa score were 0.973 and 0.955, respectively (Table 2), and had only one misclassification in the confusion matrix (Figure 6a). The out-of-bag accuracy score, drawing from pixels that weren't used in the random forest model's training phase, was 0.935. The WorldView-2 image generally scored in the mid-high 0.9s for each metric (Table 2), but did have some errors within the confusion matrix (Figure 6b) between the live *Phragmites* and native vegetation classes, as noted previously. All of the metrics for the UAS image were in the low-mid 0.9s (Table 2), indicating strong performance. It had several errors in the confusion matrix (Figure 6c), but the numbers were still small relative to the total number of pixels, resulting in good scores for user's and producer's accuracy (both above 0.91).

The visual classification differences are expected for such a complex wetland scene, but the uniformly high accuracy scores indicate that the training/validation data samples were likely unambiguous and easy to classify. This is probably related to the fact that randomly-sampled ground reference land cover data were not available for the scene. Because the reference data were created through visual interpretation of high-resolution imagery, the training/validation polygons were likely biased toward "clean" samples that were easy for the machine-learning

model to classify. This effect likely contributed to the unusually high accuracy scores seen in the study.

Another important factor contributing to the high scores is related to pixel resolution. Because the reference polygons are converted to raster format on each image's grid, differences in resolution between the platforms resulted in a large discrepancy in the number of pixels available to train and validate the random forest model (Figure 7; Table 3). In the sample polygon shown in Figure 7, the Sentinel-2 reference polygon was comprised of only 5 pixels, while the UAS reference polygon was comprised of 3,636 pixels. Ultimately, this may result in an advantage for the coarser resolution platform (Sentinel-2), because it has fewer opportunities to be penalized for incorrect classifications (Table 3). This is particularly true when the validation data are already expected to consist of relatively clear-cut samples, as discussed above. On the other hand, if Sentinel-2 did have a misclassification, it took a large hit in accuracy due to the small validation pixel count. This was the case for its user's accuracy of the live Phragmites class, where it missed just one pixel and its score dropped to 0.875 (Figure 6a).

These caveats must be considered when reviewing the objective metrics, which shouldn't solely be relied upon when assessing the classification performance in this study. While the Sentinel-2 image had very good objective metrics, its large objects and class regions fail to adequately capture the resolution on which wetland vegetation varies. Subjectively, WorldView-2 appears to have the most probable and coherent classification, with the best representation of dead *Phragmites* in previously-treated areas. In the case, the objective metrics tend to support its superior performance. The UAS results are much less coherent, but its higher resolution may capture pockets of water and native emergent vegetation better than the other two platforms. All platforms appear to over-classify live *Phragmites* and may have difficulty distinguishing it from other forms of live wetland vegetation. Generally speaking, both higher spatial resolution and additional wavelength bands appear to improve image classification, which should be one of the primary takeaways from this study.

Finally, using the random forest classifier presents the opportunity to understand which variables were most important in determining the class of image objects. These results are shown in the variable importance plots in Figure 8, providing some insight into the machine learning model. Earlier classification attempts indicated that the texture measures had very little importance (when using a 7x7 window in the calculation), so they were not used in the final random forest model for any platform. The other calculated indices proved quite helpful for the platforms with a near infrared band. The NDWI was the most important variable for both the Sentinel-2 and WorldView-2 platforms and NDVI was second-most important for WorldView-2. The multispectral bands were also very useful in determining land cover class. The red edge and near infrared bands were 2-3 in ranking (of 7) for Sentinel-2, while the near infrared band was 3rd for WorldView-2, only behind the calculated indices. The visible bands were generally less important, with blue wavelengths being the least important for WorldView-2 and the UAS. This underscores the importance of using a multispectral sensor to achieve the best results in classifying wetland vegetation.

Conclusion

Overall, the methods employed in this study produced reasonable land cover classification results and successfully generated a shapefile identifying *Phragmites* boundaries from an automated workflow. However, several limitations existed that prevent strong conclusions from being drawn, including:

- Ground reference vegetation and land cover data were not available; therefore, training and validation data were derived through visual interpretation of high-resolution imagery.
- Asynchronous images were assumed to be collected at the same time and the same set of reference data was used on images from all platforms.
- Image resolution differences resulted in a large discrepancy between platforms in the number of pixels available to train and validate the random forest model. This limits the validity of strictly using the objective metrics to assess classification performance.

With these limitations in mind, the model and workflow could be improved if ground truth reference data were gathered with a random sampling strategy at the same time the imagery was collected. This would limit the temporal discrepancy in this study and remove the subjectivity of generating reference data through visual image interpretation.

While this project generated useful results, the script and methods were designed as a prototype that could be built upon for future improvements. Image and data availability restricted the results and a limited study period prevented additional parameter optimization in the texture measure calculations, image segmentation, and random forest algorithms. The following improvements are recommended for future work:

- Collect ground reference data at the time of imagery collection
- Employ a 5-band multispectral sensor to gather high-resolution UAS imagery in red, green, blue, red edge, and near infrared wavelengths
- Experiment with the number of land cover classes used in the classification
- Perform additional optimizations to the image segmentation and random forest algorithms

Acknowledgements

Buck Ehler, Michelle Baragona, and Keith Hambrecht at the Utah DNR-FFSL were a tremendous help to this study. They provided a wealth of background information and guidance throughout the project, which shaped its focus and direction. Nate Elwood at PMG Vegetation was also very helpful for providing UAS Imagery and additional *Phragmites* spraying information. Finally, Dr. Phoebe McNeally at the University of Utah was instrumental in giving general project guidance and feedback over the course of the semester.

References

Michigan Department of Natural Resources, Wildlife Division. (2014). A guide to the control and management of invasive *Phragmites*. Retrieved from https://www.michigan.gov/documents/deq/wrd-ais-guide-phragmites_622427_7.pdf

Utah State University Utah Water Research Laboratory. (n.d.). Managing water to improve wetland functions and ecosystems. Retrieved from https://uwrl.usu.edu/water-resources/projects/wetlands

Lantz, Nicholas J. (2012). *Detection and mapping of Phragmites australis using high resolution multispectral and hyperspectral satellite imagery* (Master's Thesis). Electronic Thesis and Dissertation Repository. Retrieved from https://ir.lib.uwo.ca/etd/1012

Long, A., Kettenring, Karin M., Hawkins, Charles, Neale, Christopher, & Toth, Richard. (2014). *Distribution and drivers of a widespread, invasive wetland grass, Phragmites australis, in Great Salt Lake wetlands* (Master's Thesis). Retrieved from ProQuest Dissertations and Theses.

Sathishkumar Samiappan, Gray Turnage, Lee Allen Hathcock & Robert Moorhead (2017) Mapping of invasive *Phragmites* (common reed) in Gulf of Mexico coastal wetlands using multispectral imagery and small unmanned aerial systems. *International Journal of Remote Sensing*, 38:8-10, 2861-2882, DOI: 10.1080/01431161.2016.1271480

Caiyun Zhang, Sara Denka & Deepak R. Mishra (2018). Mapping freshwater marsh species in the wetlands of Lake Okeechobee using very high-resolution aerial photography and lidar data. *International Journal of Remote Sensing*, 39:17, 5600-5618, DOI: 10.1080/01431161.2018.1455242

PMG Vegetation. (2017, September 30). *Phragmites* Spraying [Video file]. Retrieved from https://www.youtube.com/watch?v=8JuxJi3Cq84

Vedaldi A., Soatto S. (2008). Quick shift and kernel methods for mode seeking. In: Forsyth D., Torr P., Zisserman A. (eds) *Computer Vision* – ECCV 2008. ECCV 2008. Lecture Notes in Computer Science, vol 5305. Springer, Berlin, Heidelberg

Breiman, L. (2001). *Machine Learning*, 45: 5. https://doi.org/10.1023/A:1010933404324

Figure 1. Image of *Phragmites* along the Great Salt Lake.

Figure 2. Image of *Phragmites* spraying operation by PMG Vegetation (PMG Vegetation, 2017).

	Sentinel-2	DigitalGlobe WV-2	UAS
Spectral Bands	13	8	3
Spatial Resolution	10 m	1.9 m	0.5 m
Image Dimensions	247 x 231	893 x 1276	4433 x 6421
Total Pixels	57,057	1.14 million	28.46 million

Table 1. Remote sensing imagery platforms used in study and their attributes.

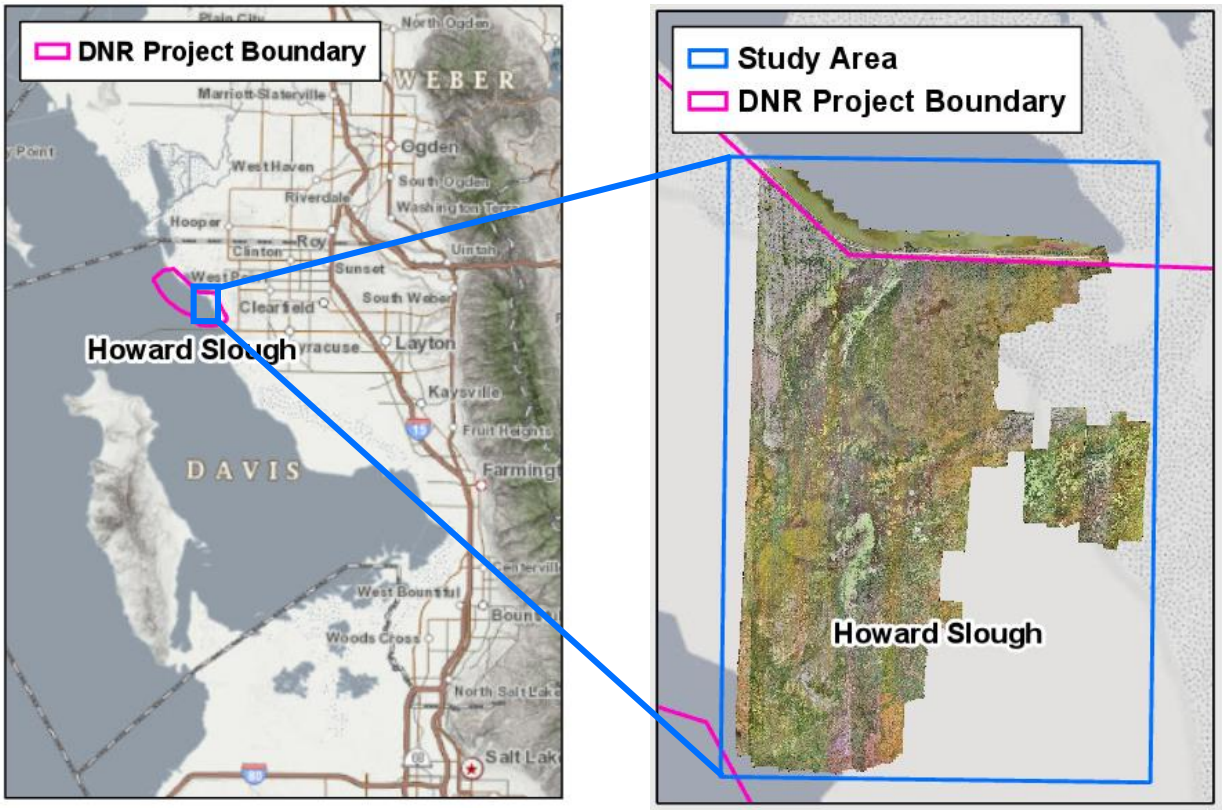

Figure 3. Reference map of Howard Slough *Phragmites* mitigation area (left) and study area for this project, including the UAS imagery footprint (right).

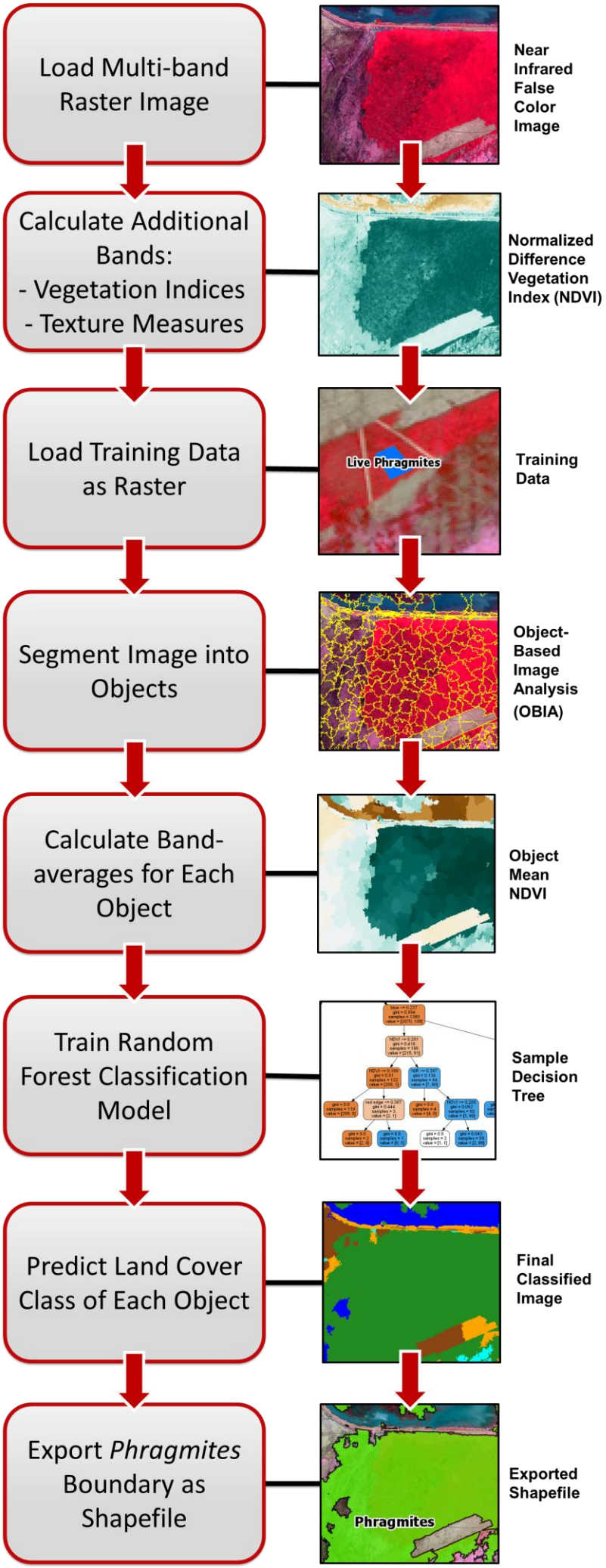

Figure 4. Diagram of automated script workflow. The left column breaks down the script into its primary functions, the right column represents a snapshot of each function's output.

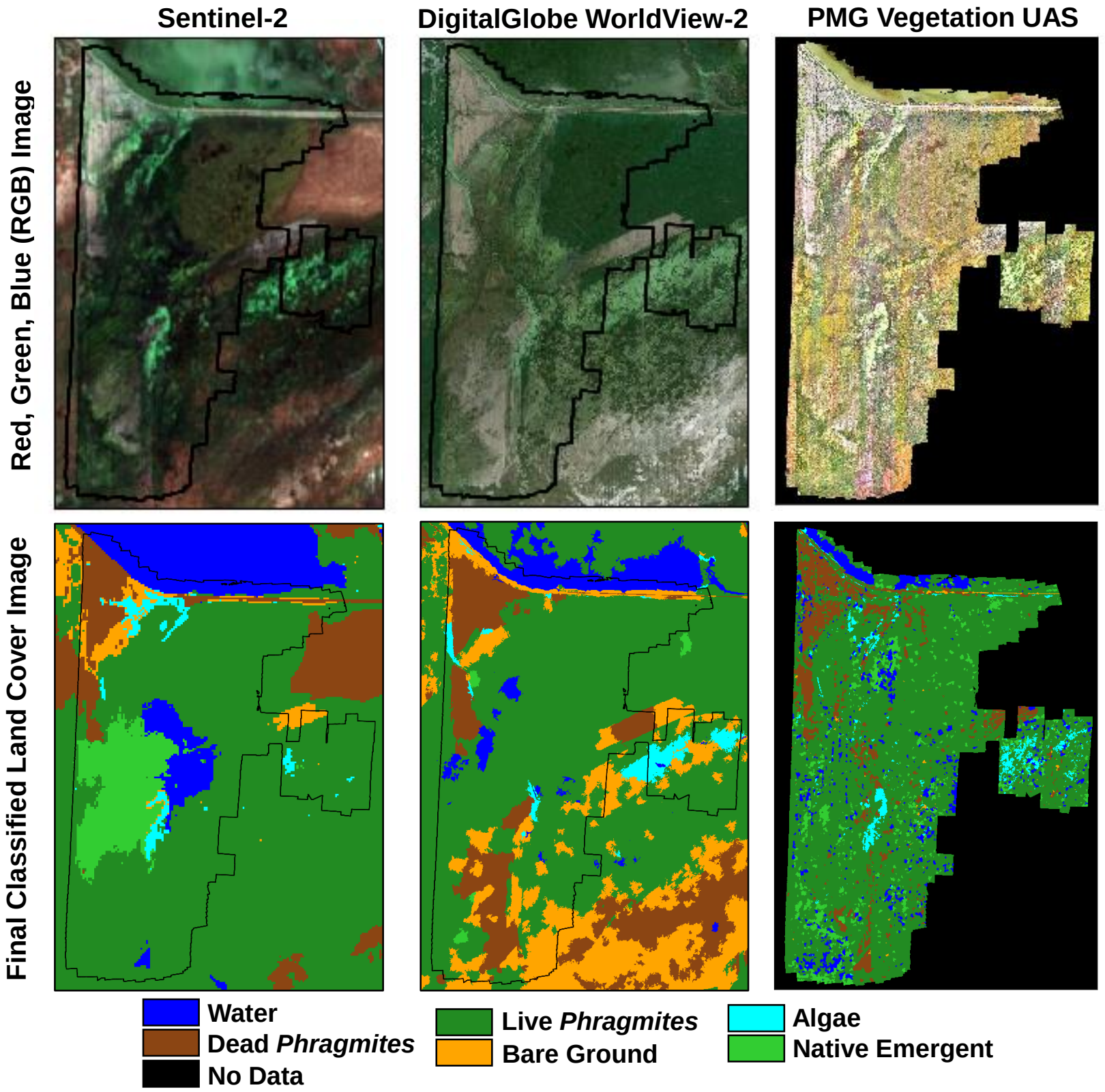

Figure 5. Standard red, green, blue (RGB) image from each platform (top row) and final classified land cover image using object-based random forest model (bottom row).

Sentinel-2 Confusion Matrix

(a)

		Predicted Label							
		Water	Live Phrag	Algae	Dead Phrag	Bare Ground	Native Emergent	Row Total	**Producer's Accuracy**
True Label	Water	20	0	0	0	0	0	**20**	1.0000
	Live Phrag	0	7	0	0	0	0	**7**	1.0000
	Algae	0	0	1	0	0	0	**1**	1.0000
	Dead Phrag	0	0	0	6	0	0	**6**	1.0000
	Bare Ground	0	0	0	0	1	0	**1**	1.0000
	Native Emergent	0	1	0	0	0	1	**2**	0.5000
	Column Total	**20**	**8**	**1**	**6**	**1**	**1**	37	
	User's Accuracy	1.0000	0.8750	1.0000	1.0000	1.0000	1.0000		

WorldView-2 Confusion Matrix

(b)

		Predicted Label							
		Water	Live Phrag	Algae	Dead Phrag	Bare Ground	Native Emergent	Row Total	**Producer's Accuracy**
True Label	Water	543	0	0	0	0	0	**543**	1.0000
	Live Phrag	0	189	1	0	0	3	**193**	0.9793
	Algae	0	0	23	0	0	0	**23**	1.0000
	Dead Phrag	0	0	0	106	2	0	**108**	0.9815
	Bare Ground	0	2	0	2	37	0	**41**	0.9024
	Native Emergent	0	13	0	0	0	17	**30**	0.5667
	Column Total	**543**	**204**	**24**	**108**	**39**	**20**	938	
	User's Accuracy	1.0000	0.9265	0.9583	0.9815	0.9487	0.8500		

UAS Confusion Matrix

(c)

		Predicted Label							
		Water	Live Phrag	Algae	Dead Phrag	Bare Ground	Native Emergent	Row Total	**Producer's Accuracy**
True Label	Water	13662	107	0	0	0	11	**13780**	0.9914
	Live Phrag	163	4481	8	83	3	142	**4880**	0.9182
	Algae	1	15	564	1	0	0	**581**	0.9707
	Dead Phrag	1	92	0	2807	18	0	**2918**	0.9620
	Bare Ground	0	4	0	30	893	0	**927**	0.9633
	Native Emergent	17	201	0	0	0	497	**715**	0.6951
	Column Total	**13844**	**4900**	**572**	**2921**	**914**	**650**	23801	
	User's Accuracy	0.9869	0.9145	0.9860	0.9610	0.9770	0.7646		

Figure 6. Confusion matrix results, user's and producer's accuracies for each land cover class for (a) Sentinel-2, (b) WorldView-2, and (c) UAS images.

Metric	S-2	DG WV-2	UAS
Overall Accuracy	0.9730	**0.9876**	0.9623
Cohen's Kappa	0.9551	0.9611	**0.9693**
Live *Phrag*. User's Accuracy	0.8750	**0.9265**	0.9145
Live *Phrag*. Producer's Accuracy	**1.0**	0.9793	0.9182
Out-of-bag Accuracy	0.9346	**0.9819**	0.9779

Table 2. A sample of accuracy metrics for each platform's final classification. Metrics are calculated from independent validation pixels that were not used to train the model.

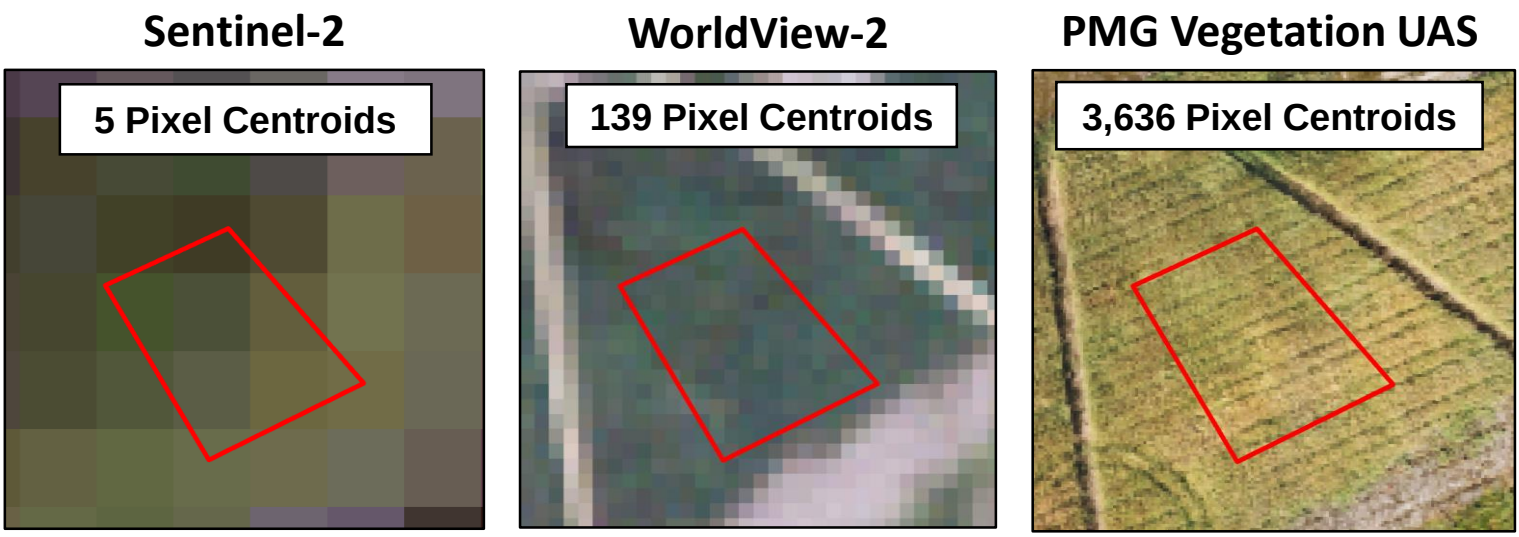

Figure 7. Example training/validation polygon (red outline) overlaid on RGB imagery from each platform to demonstrate the difference in the number pixels available for training and validation across platforms.

	S-2	DG WV-2	UAS
Total Training Pixels	99	2,811	71,403
Total Validation Pixels	33	937	23,801

Table 3. Number of training and validation pixels for each imagery platform.

(a)

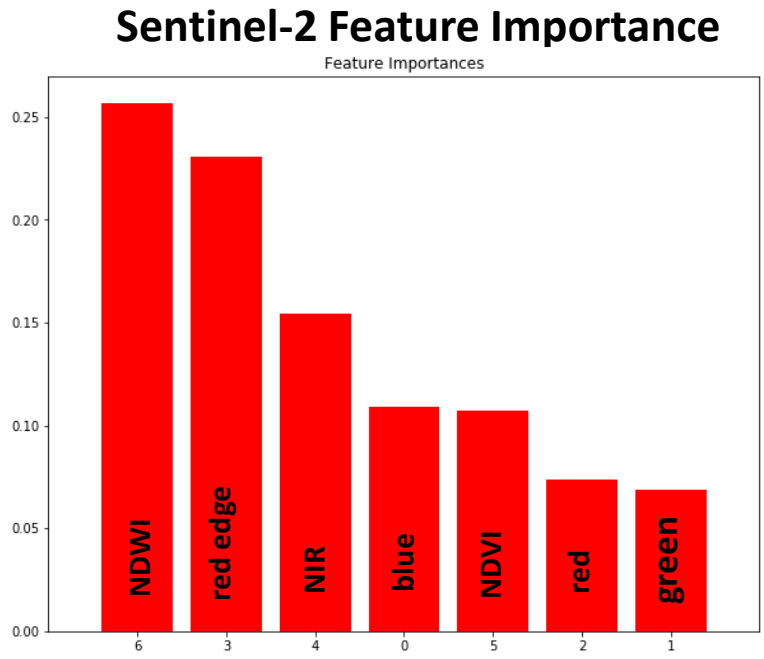

(b)

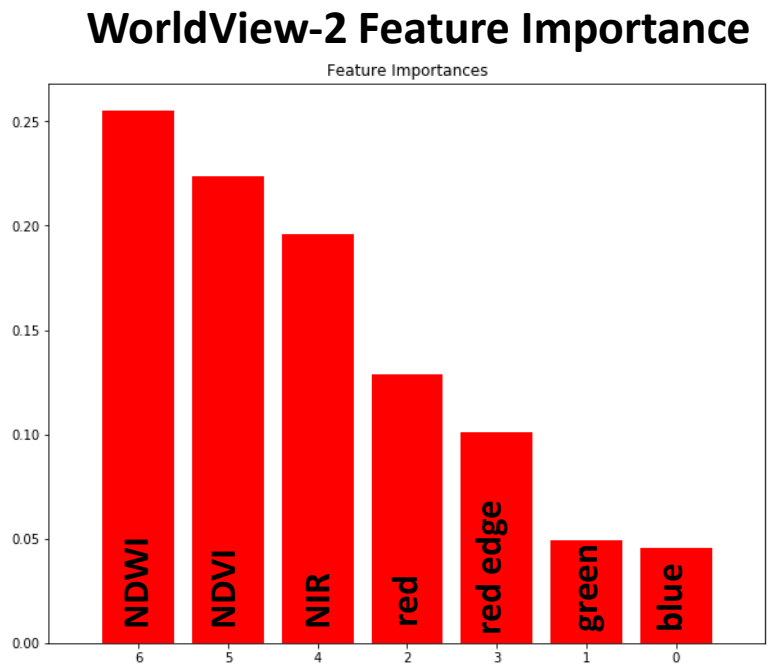

(c)

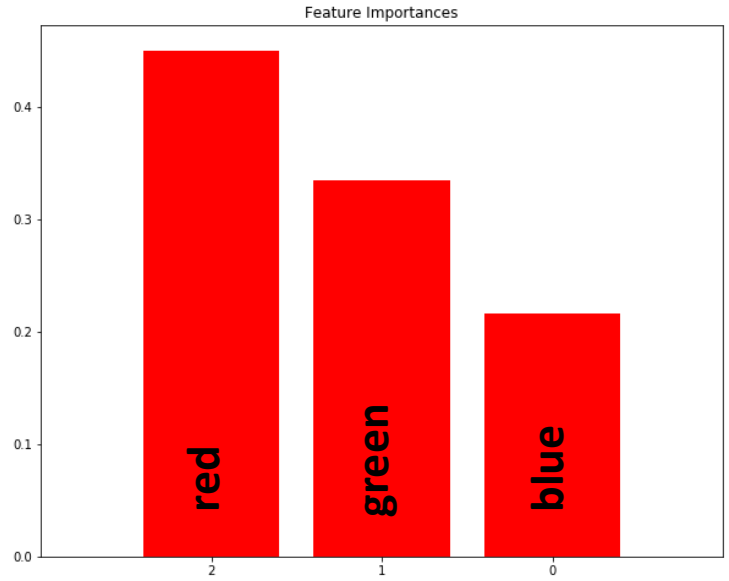

Figure 8. Feature importance plots with each image band for (a) Sentinel-2, (b) WorldView-2, and (c) UAS images.